



Transverse elasticity of a unidirectionally reinforced composite with an irregular fibre arrangement: Experiments, theory and computations

A.P.S. Selvadurai^{*}, H. Nikopour

Department of Civil Engineering and Applied Mechanics, McGill University, Montréal, QC, Canada H3A 2K6

ARTICLE INFO

Article history:
Available online 31 January 2012

Keywords:
Fibre-reinforced materials
Scanning electron microscopy
Transversely isotropic elasticity properties
Representative area method
Computational methods

ABSTRACT

This paper examines the effective elasticity properties of a unidirectionally reinforced carbon fibre–polyester composite. A computational simulation of an experimentally determined fibre arrangement is used to derive the effective elasticity properties of the transversely isotropic composite. The computational estimates for the elastic constants are compared with several theoretical estimates for the effective elasticity properties that are based on regular arrangement of the reinforcing fibres, their volume fraction and the elasticity properties of the constituents.

© 2012 Elsevier Ltd. All rights reserved.

1. Introduction

Fibre-reinforced composites consist of bonded layers of unidirectionally reinforced sub-elements, which are configured to provide the optimum deformability and resistance to failure [1–4]. Although purely unidirectionally reinforced composites are rarely used as primary load carrying components, the mechanical behaviour of such elements can contribute significantly to the development of load transfer mechanisms and the integrated action required of a composite [5,6]. In idealised assessments of the effective elasticity properties of unidirectionally reinforced composites, it is invariably assumed that the spatial arrangement of fibres is regular, which enables the application of effective elasticity estimates that are usually developed by modelling the mechanics of a representative elemental cell. Experiments conducted in connection with this research and others (see e.g. [1,7,8]) indicate that the fibre arrangement in unidirectionally reinforced composites is far from regular and that the spatial positions of the fibres invariably occur in an irregular pattern. This irregularity in the spatial arrangement of the fibres can influence the estimation of the mechanical properties of the unidirectional composite, in that the effective elasticity properties will now be influenced by a Representative Area Element (RAE) of the unidirectionally reinforced composite used to model the material. In particular, the transverse mechanical behaviour of a unidirectionally reinforced element represents the weakest link in the load transfer capabilities of the composite and thus merits detailed attention, in terms of the evaluation of its deformability, damage initiation and fracture. Despite

this importance, experimental evaluations of the transverse properties of unidirectionally reinforced materials are rare and attention has mainly focused on the evaluation of deformability and failure characteristics in the fibre direction.

In this paper we estimate the elasticity properties of a unidirectionally reinforced polyester–carbon fibre composite, considering the spatial arrangements of fibres determined from Scanning Electron Microscope (SEM) studies. The SEM studies provide visual records of the arrangements of the fibres at any transverse section, which enables the accurate geometric representation of the fibre positions in the RAE. Furthermore, the availability of SEM images of the cross-sections enables the examination of the dimensions of the RAE in relation to the area of a single fibre. The SEM data, together with an image analysis, are used to construct a computational model of the RAE, which itself can have an arbitrary orientation. The computational modelling is performed using the general purpose finite element code ABAQUS™. The RAE is subjected to different modes of homogeneous straining and the computational estimates for the strain energy are used to compute the effective elasticity properties of the composite with an irregular fibre arrangement. The study is an exercise in multi-scale modelling, which has been highlighted in a number of investigations dealing with both deformability and failure assessments. For example, Gonzalez and Llorca [9] have examined the process of fracture in unidirectionally reinforced composites using multi-scaling techniques. Sansalone et al. [10] use a multi-field model to computationally examine the influence of local micro-fibre orientation on stress and strain distribution in fibre-reinforced composites. Trias et al. [11] use computational approaches to identify RAEs where the periodicity in the boundary conditions is relaxed to account for statistical influences, including clustering. The research in the

^{*} Corresponding author. Tel.: +1 514 398 6672; fax: +1 514 398 7361.
E-mail address: patrick.selvadurai@mcgill.ca (A.P.S. Selvadurai).

current paper also points to the minimum fibre area fraction necessary to ensure the validity of the idealised continuum concept in estimating the transverse elasticity properties of the composite using analytical and computational means.

2. Experimental characterisation of fibre configurations

The experimental research programme involved the study of the fibre arrangement in a cross section of a Carbon Fibre-Reinforced Plastic (CFRP) multi-laminate plate. The plate used in the research investigations was supplied by a composites products manufacturer in the USA. The supplied multi-ply plates had different thicknesses, different fibre directions in the individual plies and a relatively constant fibre volume fraction. The properties of the composite constituents (i.e. resin and fibre) in the as supplied condition were provided by the manufacturer and these are given in Table 1.

The particular objectives of the research were to examine the arrangement of fibres in a cross-section of a composite and to focus more specifically on a transverse section of the laminate containing the uni-directional fibre reinforcement. The imaging of the fibre

Table 1
Mechanical properties of resin matrix and fibre.

Property	Specific gravity	Tensile strength (MPa)	Tensile Young's modulus (GPa)	Ultimate tensile strain (%)	Poisson's ratio
Resin	1.20	78.6	3.1	3.4	0.35
Fibre	1.81	2450.4	224.4	1.6	0.20

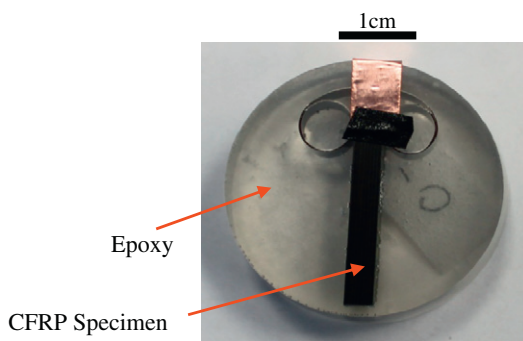


Fig. 1. Sample prepared for SEM scanning.

arrangements was performed using a SEM. Samples of the 3.6 mm thick multi-laminate CFRP plate were cut into coupon sizes measuring 25.4 mm by 5.0 mm. These were cast in epoxy that hardened within 24 h and they were then polished using silicon carbide paper (220 grits) (Fig. 1). The finishing was done using a finer silicon carbide paper (600 grits). The final polishing operation was performed with diamond solutions (15 μm and 0.05 μm). The polished samples were carbon coated with a layer of less than 30 nm, to eliminate the charging effect of the non-conductive materials used in a SEM environment.

In electron microscopy, the interaction of electrons and the material under investigation can produce different signals, including secondary, backscatter and Auger electrons, characteristic X-rays, bremsstrahlung, etc. The backscatter electron signals were used to obtain chemical information of the constituents. The theoretical procedures used in the interpretation of the SEM data are given by Goldstein et al. [12]. An Everhart-Thornley detector was used to record the secondary electrons, which are emitted from the surface of the materials. To increase the quality of the signal, the acceleration voltage of the microscope and the probe current were decreased. The tension was set to 2 kV and the current was adjusted to a low value. The backscattered electron coefficient (i.e. the ratio of the back-scattered electrons to the primary electrons) is a function of the mean atomic number of the emitted signal. The fibres in the composite have a higher mean atomic number than the surrounding matrix; thus, on the image the fibres appear brighter than the resin. Better quality backscattered electron images were obtained with a higher acceleration voltage and higher current. The voltage was set to 10 kV and the current was adjusted to a higher value. For each frame, the brightness and contrast were manually adjusted before acquisition of an image. Fig. 2 shows typical scan of an intact specimen.

The image processing toolbox in the MATLAB™ software was used to estimate the fibre volume fraction. All scans were converted into binary black and white images and filter commands were then used to eliminate noise associated with each image. The filtered binary image was then used to estimate the fibre volume fraction. The diameter of an average fibre was approximately 8 μm . Some fibres, however, had a smaller diameter although their proportions in a control region, such as the one shown in Fig. 2, did not exceed 5%. The fibre area fraction was estimated by using square sub-regions with varying dimensions of $0.5D$, $1D$, $2D$, $3D$, ..., to nD , where D is the fibre diameter and n depends on the dimensions of the photographic image. The orientation of the sub-region with respect to the global view of the image was selected at 0° and 45° (Fig. 3).

Fig. 4 illustrates the variation of the experimentally determined fibre area fraction as a function of the orientation and area of the

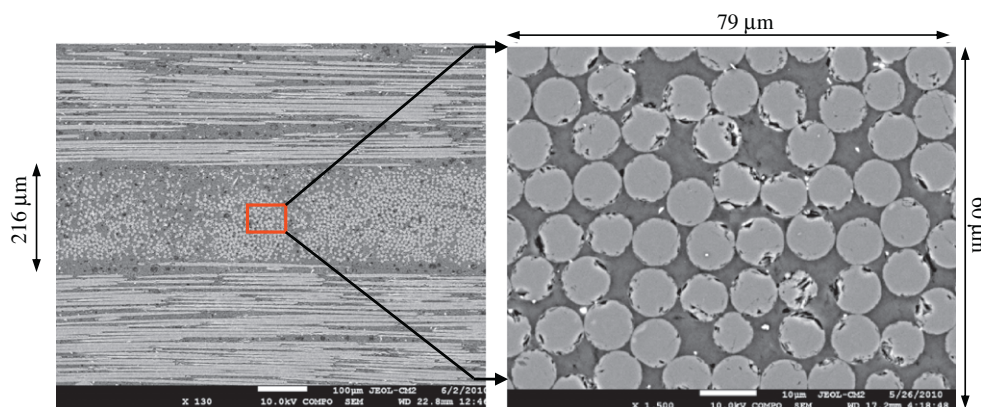


Fig. 2. Scan of the CFRP composite and a region selected for FEM analysis.

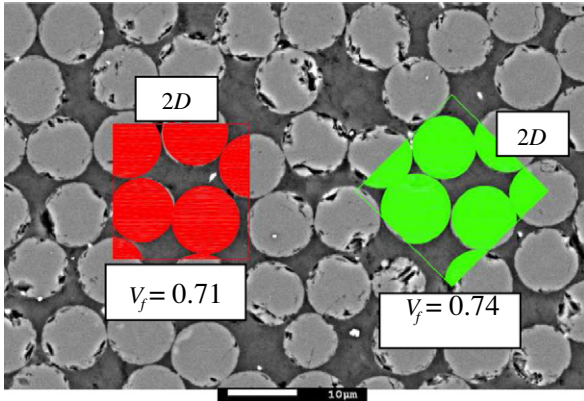


Fig. 3. Estimation of fibre area fractions using squares in two different orientations.

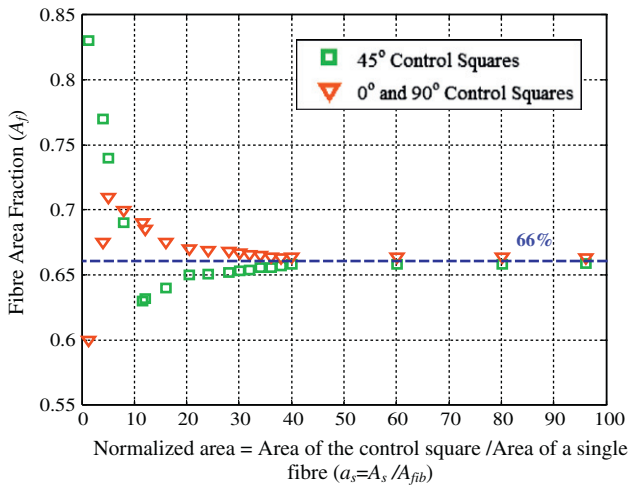


Fig. 4. Estimation of the effective fibre area fraction in orientations normal to the fibre direction; representative areas aligned at two different orientations (A_s = Area of the control square; A_{fib} = Area of individual fibre).

control region. As is evident from Fig. 4, the fibre area fraction converges approximately to 66% for the image shown in Fig. 3. Fibres were non-uniformly distributed in different layers of the laminated composite.

A series of tension tests (ASTM D3039 [13]) were also performed on single lamina strips of the composite, which measured 25.4 mm in width and 203.2 mm in effective length, to determine

the elastic properties of the composite material. The experimentally determined longitudinal Young’s modulus of a single lamina, E_{11} , was 138.26 ± 5.26 GPa; Poisson’s ratio, ν_{12} was 0.23 ± 0.01 , and the tensile strength, σ_{1T} , was 1442.5 ± 110.3 MPa, where the subscript 1 refers to the fibre direction and subscripts 2 and 3 refer to transverse directions, which together with the direction 1, form an orthogonal basis.

The bond between the fibre and the matrix is the main process that contributes to the transverse strength and deformability characteristics of the unidirectional fibre-reinforced material. This property cannot be determined from bulk tests and special interface adhesion measurements are required. Some knowledge of the load transfer characteristics of the interface or bond integrity can be gleaned by observation of the fracture topography. As is evident from Fig. 5, the failure of the fibre-reinforced material involves fibre breakage rather than fibre pull out. This points to a fibre-reinforced material with adequate fibre–matrix bond.

3. Theoretical estimates

Theoretical modelling of the elastic behaviour of unidirectionally fibre-reinforced materials has been an active topic of research over the past seven decades. The unidirectional positioning of the parallel reinforcing fibres in either a random or regular arrangement, permits the description of the overall elastic behaviour of the composite by appeal to the classical theory of elasticity for a transversely isotropic material. When the axis of symmetry of the transversely isotropic elastic material is aligned with the fibre direction, five independent elastic constants are necessary and sufficient to characterise the complete linear elastic behaviour. The general theories that relate these elastic constants to the elasticity properties of the fibres and the respective area fractions, contiguity effects, etc., are many and varied; they depend to a large extent on the assumptions used in modelling the representative element and the analytical techniques used to arrive at either a variational or other elementary analysis based on structural representations of the composite action between the fibres and the matrix. Comprehensive accounts of these developments can be found in the texts and articles by Hill [14,15], Hashin and Rosen [16], Halpin and Tsai [17], Whitney and Riley [18], Spencer [19], Sideridis [20], Sun and Vaidya [21] and accounts of recent developments can be found in the articles by Selvadurai [5,6].

3.1. Equations governing transversely isotropic elasticity behaviour

If the fibre direction is designated as 1, the equations of transversely isotropic elasticity can be written as

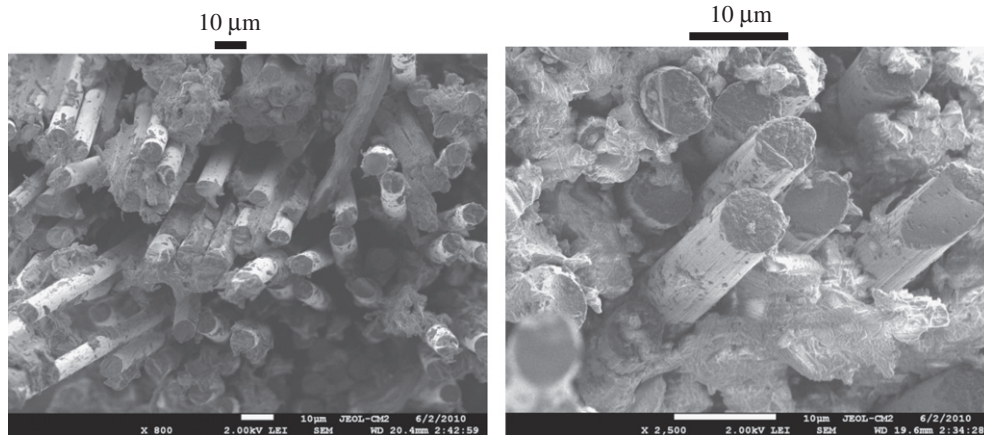


Fig. 5. The fracture topography.

$$\begin{aligned}\sigma_{11} &= C_{11}\varepsilon_{11} + C_{12}\varepsilon_{22} + C_{12}\varepsilon_{33}; & \sigma_{12} &= 2C_{66}\varepsilon_{12} \\ \sigma_{12} &= C_{12}\varepsilon_{11} + C_{22}\varepsilon_{22} + C_{23}\varepsilon_{33}; & \sigma_{23} &= (C_{22} - C_{23})\varepsilon_{23} \\ \sigma_{13} &= C_{12}\varepsilon_{11} + C_{23}\varepsilon_{22} + C_{22}\varepsilon_{33}; & \sigma_{31} &= 2C_{66}\varepsilon_{31}\end{aligned}\quad (1)$$

and the elastic constants C_{ij} can be related to the five independent measurable elastic moduli E_{11} , ν_{23} , K_{23} , G_{12} , and G_{23} as follows

$$\begin{aligned}C_{11} &= E_{11} + 4\nu_{12}^2 K_{23}; & C_{12} &= 2K_{23}\nu_{12}; & C_{22} &= G_{23} + K_{23} \\ C_{23} &= -G_{23} + K_{23}; & C_{66} &= G_{12}\end{aligned}\quad (2)$$

Also, the elastic constants in the 2–3 plane, or the plane of isotropy, are generally assumed to satisfy the usual relationships applicable to isotropic elastic materials. In the description of the elastic properties in the plane of isotropy, it is also customary to define the plane strain bulk modulus, K_{23} , which is given by

$$K_{23} = \frac{1}{2}(C_{22} + C_{33}) \quad (3)$$

The choice of the plane strain bulk modulus, K_{23} , is an idealisation, which implies that $\varepsilon_{11} = 0$. This assumption is rigorously satisfied if either $E_{11} \rightarrow \infty$ or the loading conditions of the composite ensures, through symmetry considerations, that $\varepsilon_{11} = 0$. Neither of these conditions is rigorously satisfied and the plane strain bulk modulus therefore can only be regarded as an idealisation. The in-plane shear modulus G_{23} is regarded as the second elastic constant. The other elastic constants can be related to K_{23} and G_{23} through the relationships

$$\begin{aligned}E_{22} = E_{33} &= \frac{4K_{23}G_{23}}{K_{23} + \psi G_{23}} \\ \nu_{23} &= \frac{K_{23} - \psi G_{23}}{K_{23} + \psi G_{23}}; & \nu_{21} = \nu_{31} &= \frac{1}{2} \left(\frac{C_{11} - E_{11}}{K_{23}} \right) \\ \psi &= 1 + \frac{4K_{23}\nu_{12}^2}{E_{11}}\end{aligned}\quad (4)$$

3.2. Effective elasticity parameters

Several theoretical models have been proposed in the literature for estimating the elasticity properties of unidirectionally reinforced composites. Extensive accounts of these developments can be found in the literature cited previously. Some typical estimates for the elastic constants applicable to unidirectionally reinforced composites will be presented.

3.2.1. Voigt and Reuss estimates

The simplest equations used for estimating the effective properties of a composite are the upper and lower bounds proposed by Voigt and Reuss, respectively, as given in [4]. The general relationships can be applied universally for estimating any of the elastic properties of the composite. For example the, Voigt and Reuss bounds for the effective bulk modulus K_{23} of the unidirectionally fibre-reinforced composite in the plane of symmetry can be estimated from the result

$$\frac{1}{\frac{\nu_f}{K_f} + \frac{(1-\nu_f)}{K_m}} \leq K_{23} \leq K_f \nu_f + (1 - \nu_f)K_m \quad (5)$$

where ν_f is the volume fraction of the fibres and K_f and K_m are, respectively, the bulk moduli of the fibre and matrix phases. These bounds are the simplest but not necessarily the best, since the results may vary by a wide margin depending on the volume fraction of the fibres. Similarly, other elasticity properties G_{12} , G_{13} , G_{23} , E_{11} , E_{22} , E_{33} , ν_{12} , ν_{13} , ν_{23} can be bounded by the Voigt and Reuss estimates; e.g.

$$\frac{1}{\frac{\nu_f}{E_f} + \frac{(1-\nu_f)}{E_m}} \leq E_{22} \leq E_f \nu_f + (1 - \nu_f)E_m \quad (6)$$

3.2.2. Hashin and Rosen estimates

The most widely used estimates for the elastic constants of a unidirectionally reinforced composite are due to Hashin and Rosen [16], and take the following forms:

$$K_{23} = (\lambda_m + G_m) \left\{ \frac{\zeta(1 + 2\nu_m \nu_f) + 2\nu_m V_m}{\zeta V_m + \nu_f + 2\nu_m} \right\} \quad (7)$$

$$E_{11} = \nu_f E_f + V_m E_m + \frac{4\nu_f V_m (\nu_f - \nu_m)^2 G_m}{\frac{V_m G_m}{K_f + (\frac{G_m}{3})} + \frac{\nu_f G_f}{K_f + (\frac{G_m}{3})}} \quad (8)$$

$$\nu_{12} = \nu_{13} = \left\{ \frac{\nu_f E_f L_1 + V_m E_m L_2 \nu_m}{\nu_f E_f L_3 + V_m E_m L_2} \right\} \quad (9)$$

$$G_{12} = G_{13} = G_m \left\{ \frac{\eta(1 + \nu_f) + V_m}{\eta V_m + \nu_f + 1} \right\} \quad (10)$$

and

$$G_{23} = G_m \left\{ \frac{(\alpha + \beta_m \nu_f)(1 + \rho \nu_f^3) - 3\nu_f V_m^2 \beta_m^2}{(\alpha - \nu_f)(1 + \rho \nu_f^3) - 3\nu_f V_m^2 \beta_m^2} \right\} \quad (11)$$

where

$$\begin{aligned}\lambda_i &= \frac{\nu_i E_i}{(1 + \nu_i)(1 - 2\nu_i)}; & \beta_i &= (3 - 4\nu_i)^{-1}; & (i = m, f) \\ \zeta &= \left(\frac{\lambda_f + G_f}{\lambda_m + G_f} \right); & \alpha &= \left(\frac{\eta + \beta_m}{\eta - 1} \right); & \rho &= \left(\frac{\beta_m - \eta \beta_f}{1 + \eta \beta_f} \right); & \eta &= \frac{E_f(1 + \nu_m)}{E_m(1 + \nu_f)} \\ L_1 &= 2\nu_f(1 - \nu_m^2) + V_m \nu_m(1 + \nu_m); & L_2 &= 2\nu_f(1 - \nu_f^2) \\ L_3 &= 2\nu_f(1 - \nu_m^2)\nu_f + V_m(1 + \nu_m)\end{aligned}\quad (12)$$

It should be noted that the model for the composite used by Hashin and Rosen [16] assumes that the fibres are surrounded by a matrix material, thereby ensuring non-contiguity between adjacent fibres. In the experimental evaluations conducted in connection with this research, it was observed that there is a spatial variation in the contiguity factor, which can influence the assessment of the effective transverse elasticity properties.

3.2.3. Halpin and Tsai estimates

Halpin and Tsai [17] used an interpolation procedure to estimate elasticity properties of a unidirectionally fibre-reinforced composite:

$$\begin{aligned}E_{11} &= (1 - L) \frac{K_f E_f (2K_m + G_m) - K_m E_m (K_f - G_m) V_m}{K_f (2K_m + G_m) - G_m (K_f - K_m) V_m} \\ &+ L \frac{K_f E_m (2K_f + G_f) V_m + K_f E_f (K_m - G_m) \nu_f}{K_f (2K_m + G_f) - G_f (K_m - K_f) V_m}\end{aligned}\quad (13)$$

$$\begin{aligned}\nu_{12} &= (1 - L) \frac{K_f \nu_f (2K_m + G_m) - K_m \nu_m (K_f - G_m) V_m}{K_f (2K_m + G_m) - G_m (K_f - K_m) V_m} \\ &+ L \frac{K_f \nu_m (2K_f + G_f) V_m + K_f \nu_f (K_m - G_m) \nu_f}{K_f (2K_m + G_f) - G_f (K_m - K_f) V_m}\end{aligned}\quad (14)$$

where L is defined as the contiguity factor,

$$E_{22} = E_m \frac{1 + \xi \eta \nu_f}{1 - \eta \nu_f} \quad (15)$$

$$\nu_{23} = \nu_m \frac{1 + \xi \eta \nu_f}{1 - \eta \nu_f} \quad (16)$$

$$G_{12} = G_m \frac{1 + \xi\eta V_f}{1 - \eta V_f} \quad (17)$$

and ξ and η depend on fibre and matrix elasticity, geometry, packing condition and loading patterns.

3.2.4. Whitney and Riley estimates

Whitney and Riley [18] presented estimates for the elastic constants of a unidirectionally fibre-reinforced elastic matrix. These developments are based on structural mechanics models of the representative elements and are less rigorous than the procedures developed by Hill, Hashin and Rosen and others [14–16], which are based on variational theorems in elasticity. These authors also present the results of experiments and comparisons with experimental results conducted on an epoxy resin reinforced with boron fibres. The expressions for the elasticity constants can be deduced from the expressions given below by Whitney and Riley [18] and the results (1)–(4):

$$K_{23} = \frac{[(K_f + G_m)K_m - (K_f - K_m)G_m V_f]}{[(K_f + G_m) - (K_f - K_m)V_f]} \quad (18)$$

$$E_{11} = V_f(E_f - E_m) + V_m E_m \quad (19)$$

$$G_{23} = \frac{[(G_f + G_m) + (G_f - G_m)G_m V_f]}{[(G_f + G_m) - (G_f - G_m)V_f]} \quad (20)$$

$$\nu_{23} = V_f \nu_f + V_m \nu_m \quad (21)$$

$$\nu_{12} = \nu_m - \frac{2(\nu_m - \nu_f)(1 - \nu_m)^2 E_f V_f}{E_m(1 - V_f)L_1 + E_f[V_f L_2 + (1 + \nu_m)]} \quad (22)$$

where;

$$L_1 = 1 - \nu_f - \nu_f^2 \quad (23)$$

$$L_2 = 1 - \nu_m - \nu_m^2 \quad (24)$$

4. Computational modelling

An objective of the research was to use the information on the fibre configurations, derived from SEM scans, to develop a geometric model of the fibre arrangement in the composite which can be used to computationally estimate the effective elasticity properties.

4.1. Finite element models

The computational modelling was performed using the ABAQUS™ software. Finite element models of the representative area elements were constructed using the images derived from the SEM scans (Fig. 6) and these elemental regions were subjected to appropriate states of homogeneous strain to estimate, through energy equivalence, the effective elasticity properties of the composite. These computational estimates for the effective elasticity properties for unidirectionally fibre-reinforced composites with an irregular fibre arrangement were then be compared with computational results and analytical estimates for an ideal unidirectionally fibre-reinforced composite with the same fibre volume fraction and fibre diameter.

Transverse properties, including the plane strain bulk modulus, K_{23} ; the plane strain shear modulus, G_{23} ; the transverse Young's modulus, E_{22} , and Poisson's ratio, ν_{23} , were identified using two-dimensional plane strain models. The longitudinal properties, including the longitudinal Young's modulus, E_{11} , and Poisson's ratio, ν_{12} , were predicted using three-dimensional models. Discretizations of two-dimensional models were performed using the standard

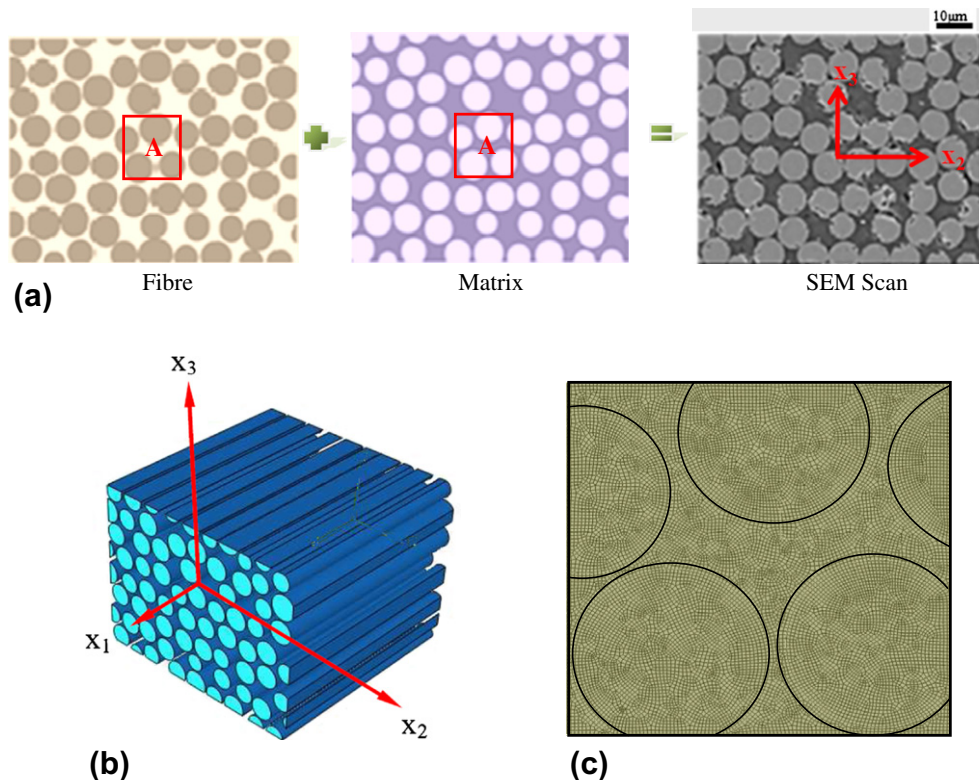


Fig. 6. FEM Computational models for identification of: (a) Transverse properties (two-dimensional), (b) longitudinal properties (three-dimensional), and (c) Finite element mesh (detail at A) (Number of elements: 12,251, Element type: 4-node bilinear quadrilateral).

4-node bilinear quadrilateral element available in ABAQUS™ (CPS4R), and for discretization of three-dimensional models, a 4-node linear tetrahedron element (C3D4) was used. Perfect bonding between the matrix and fibres was assumed and damage effects that can result from matrix cracking, debonding at the fibre–matrix interface, transverse cracking of fibres and other defects were not considered in these models. The fibres and the matrix were modelled as isotropic materials having elastic constants indicated in Table 1. Details of boundary conditions and constraints for identification of each elasticity property, along with the energy density equation for a homogenous transversely isotropic section under the same boundary conditions and constraints, are presented in the following sections. Stress and strain distributions were achieved and the strain energy density of the Representative Area Element (RAE) was calculated using the general equation for arbitrary heterogeneous isotropic materials [5,22].

$$U = \frac{1}{2V} \iiint_V \{\underline{\sigma}\}^T \{\underline{\epsilon}\} dV \quad (25)$$

4.2. Boundary conditions and constraints

4.2.1. Plane strain bulk modulus, K_{23}

The state of strain chosen to be applied to RAEs to computationally estimate K_{23} was

$$\epsilon_{22} = \epsilon_{33} = \epsilon_0; \quad \epsilon_{11} = 0; \quad \epsilon_{12} = \epsilon_{13} = \epsilon_{23} = 0 \quad (26)$$

By employing the plane strain conditions for an isotropic material, the strain energy density expression can be simplified and restated in terms of the effective bulk modulus as

$$U = 2K_{23}\epsilon_0^2 \quad (27)$$

ϵ_0 was chosen to be 0.01 for all RAEs with different dimensions.

4.2.2. Plane strain shear modulus, G_{23}

The state of strain associated with the plane strain shear modulus, G_{23} , was chosen as pure shear in the x_2x_3 plane (the coordinate system is shown in Fig. 6).

$$\epsilon_{11} = \epsilon_{22} = \epsilon_{33} = 0; \quad \epsilon_{23} = \epsilon_{32} = \gamma_0; \quad \epsilon_{13} = 0 \quad (28)$$

For prescribed boundary conditions, the macroscopic strain energy density for an isotropic material can be expressed as:

$$U = \frac{1}{2} G_{23} \gamma_0^2 \quad (29)$$

and γ_0 was chosen to be 0.01.

4.2.3. Transverse Young's modulus E_{22} and Poisson's ratio, ν_{23}

The following boundary conditions were proposed for RAEs to estimate the effective transverse Young's modulus, E_{22} , and Poisson's ratio, ν_{23} . The RAE was subjected to known displacements, $\epsilon_0 L$, along an axis for the case when straining is in the x_2 -direction.

$$\epsilon_{11} = 0; \quad \epsilon_{22} = \epsilon_0; \quad \epsilon_{12} = \epsilon_{13} = \epsilon_{32} = 0 \quad (30)$$

The following displacement boundary conditions were imposed on the unstressed sides of the models to ensure the homogeneity of the deformation:

$$U_3(X, Y, H/2) = U_3(X, W/2, H/2) \quad (31)$$

$$U_3(X, Y, -H/2) = U_3(X, W/2, -H/2) \quad (32)$$

where W and H are the dimensions of the selected area elements.

The transverse Poisson's ratio, ν_{23} was calculated using the values of the strains observed in the transverse direction and the imposed axial strain, i.e.

$$\nu_{23} = \frac{-\epsilon_{33}}{\epsilon_{22}} \quad (33)$$

For the proposed boundary conditions, the strain energy density for an isotropic material can be expressed as:

$$U = \frac{E_{22}}{2(1 + \nu_{23})(1 - 2\nu_{23})} [(1 - \nu_{23})(\epsilon_{22}^2 + \epsilon_{33}^2) + 2\nu_{23}\epsilon_{22}\epsilon_{33}] \quad (34)$$

4.2.4. Longitudinal Young's modulus, E_{11} , and Poisson's ratio, ν_{12}

The cuboidal specimen was subjected to the following state of strain:

$$\epsilon_{11} = \epsilon_0; \quad \epsilon_{13} = \epsilon_{23} = \epsilon_{32} = 0 \quad (35)$$

The displacement constraints applied on the lateral surfaces of the model to ensure homogenous displacement of the control element were

$$\begin{aligned} U_3(X, Y, H/2) &= U_3(X, W/2, H/2) \\ U_3(X, Y, -H/2) &= U_3(X, W/2, -H/2) \\ U_2(X, W/2, Z) &= U_2(X, W/2, H/2) \\ U_2(X, -W/2, Z) &= U_2(X, -W/2, H/2) \end{aligned} \quad (36)$$

The longitudinal Poisson's ratio can be estimated by dividing the strain observed in the lateral surfaces to the applied strain in the fibre direction:

$$\nu_{12} \approx \nu_{13} \approx \frac{-\epsilon_{22}}{\epsilon_{11}} \approx \frac{-\epsilon_{33}}{\epsilon_{11}} \quad (37)$$

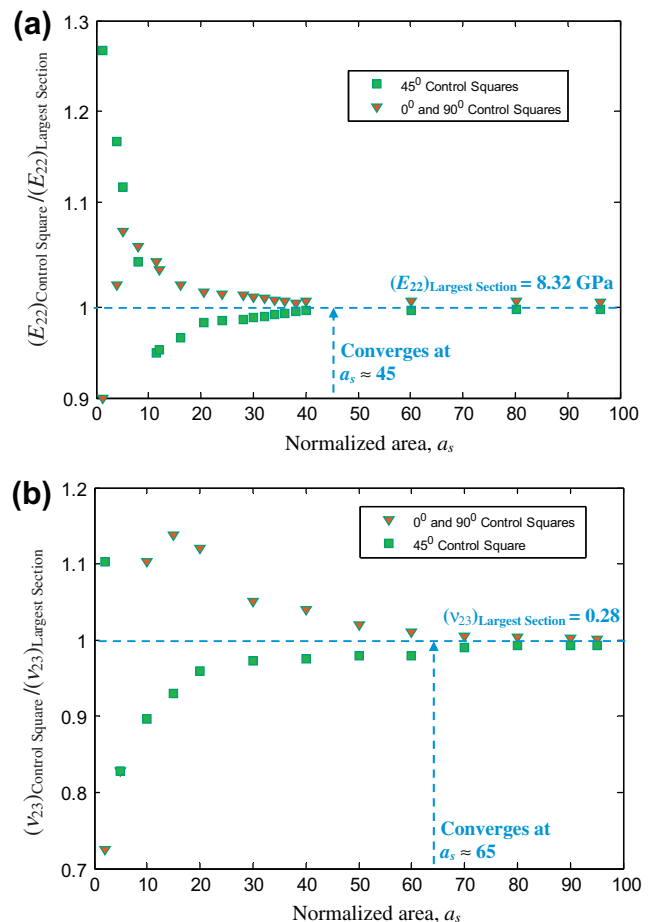


Fig. 7. Normalised estimates of the transverse elasticity properties: (a) Young's modulus, E_{22} and (b) Poisson's ratio, ν_{23} .

The macroscopic strain energy density function for the equivalent isotropic material therefore reduces to:

$$U = \frac{1}{2} E_{11} \epsilon_0^2 \tag{38}$$

5. Results and discussion

Computational models were developed for square sub-regions of cross sections of a composite with random fibre arrangements, with dimensions $0.5D, 1D, 2D, 3D, \dots, nD$, where D is the fibre diameter. The orientation of the sub-region with respect to the global view of the image of the fibre-reinforced composite generated from a SEM scan was selected at 0° and 45° . A similar model was developed for a section with an idealised regular fibre arrangement corresponding to the same fibre volume fraction and fibre diameters. As the area of the RAE increased, results for the elasticity properties of the control squares with the random fibre arrangements converged to the values of the composite block with a regular fibre arrangement. Fig. 7 illustrates that normalised transverse elastic modulus, $[(E_{22})_{\text{Control Square}} / (E_{22})_{\text{Largest Section}}]$, and normalised Poisson's ratio, $[(\nu_{23})_{\text{Control Square}} / (\nu_{23})_{\text{Largest Section}}]$, for the CFRP sections versus normalised area of the control squares, $a_s = A_s / A_{\text{fib}}$. Based on the results for the CFRP section examined in this paper, it can be concluded that the transverse Poisson's ratio, ν_{23} , is more sensitive to the irregular fibre arrangement (i.e. convergence at $a_s \approx 65$) compared to the transverse Young's modulus, E_{22} , (i.e. convergence at $a_s \approx 45$).

Figs. 8–10 illustrate the stress and/or strain distributions resulting from the various boundary conditions discussed in the previous section for the RAE; the results are for the scan where the control area in relation to the fibre area is the largest ($a_s \approx 100$). In the

model to identify the transverse bulk modulus, K_{23} (Fig. 8) the magnitude of the von Mises stress was considerably lower in those areas with low fibre densities compared to the areas with a higher fibre density. In the model for the identification of the transverse Young's modulus (Fig. 9) the magnitude of the strain, ϵ_{22} , in the fibres was much lower than that in the matrix; however, the von Mises stress showed a more uniform distribution in the composite section. The maximum magnitude of the von Mises stress was observed in the locations where the composite contained a higher fibre density.

The stress distribution in the model developed to identify the transverse shear modulus, G_{23} , is presented in Fig. 10a. In the shear model, the maximum von Mises stress was observed in the corner with the highest fibre density, whereas the minimum von Mises stress was observed on the mid-side with the lowest fibre density. In the three-dimensional model used in the computational estimation of the longitudinal properties (Fig. 10b), the longitudinal strain, ϵ_{11} , was identical in both the fibre and matrix, irrespective of the fibre arrangement and the area of the transverse section.

Table 2 summarizes the values of the elasticity properties, calculated using theoretical relationships and Representative Area Element (RAE) methods for the largest representative area. Computational results for the properties of the largest block with both the irregular fibre arrangement and the regular fibre arrangement were almost identical. It was also noted that the analytical results of Hashin and Rosen [16], which are based on rigorous energy variational principles in mechanics, provided the closest correlation for the elasticity properties in comparison to those derived using the RAE technique for the relatively large RAE. However, the differences between the theoretical estimates and the RAE approach decreased as the size of the RAE increased in comparison to the area of the fibre.

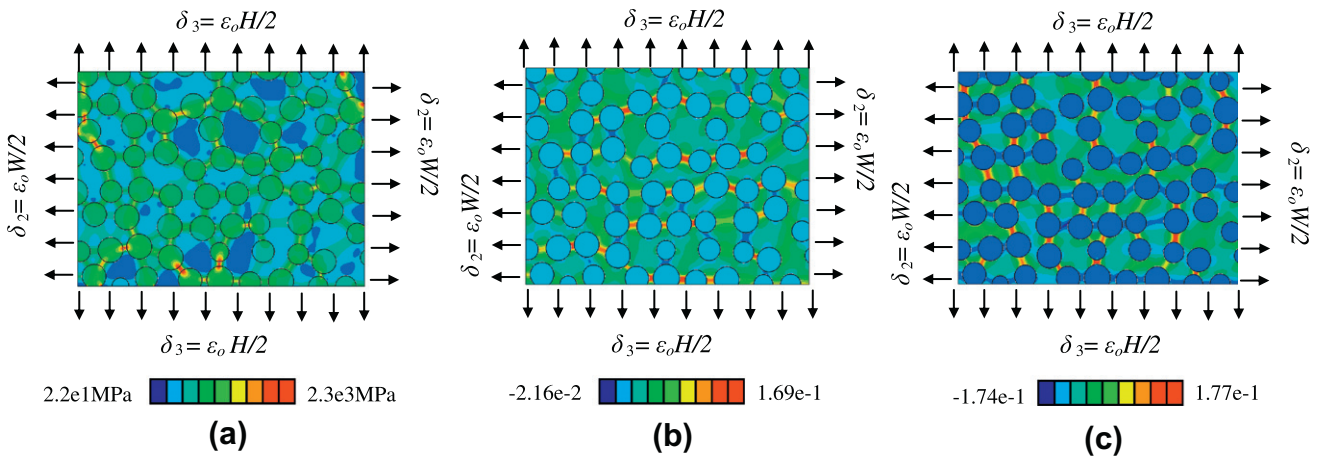


Fig. 8. Bulk modulus, K_{23} , model: (a) Stress, σ_{vonMises} , (b) Strain, ϵ_{22} , and (c) Strain, ϵ_{33} .

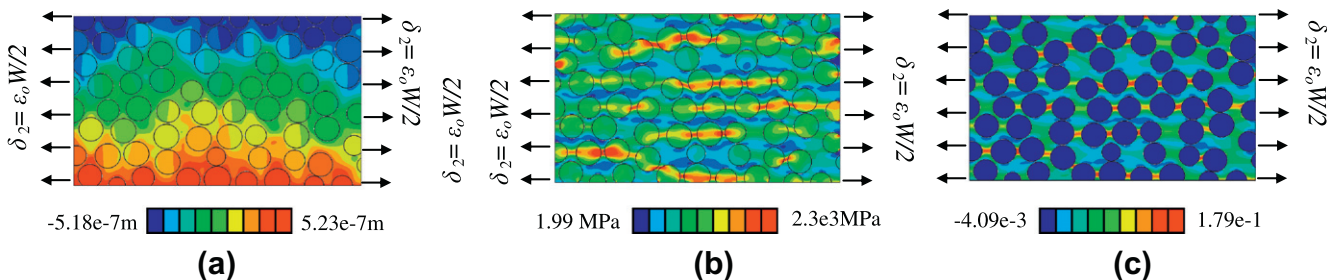


Fig. 9. Transverse Young's modulus, E_{22} , and Poisson's ratio, ν_{23} , model: (a) the deformation, U_3 , (b) Stress, σ_{vonMises} , and (c) Strain, ϵ_{22} .

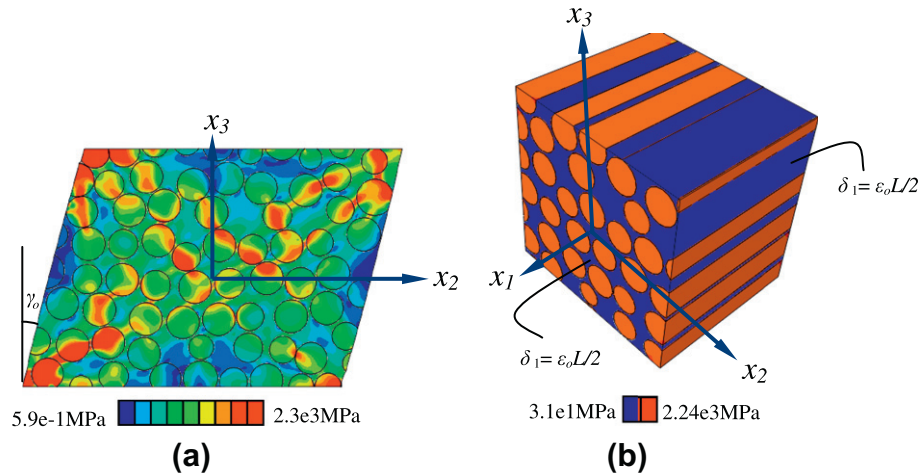


Fig. 10. Stress distribution, $\sigma_{vonMises}$, in the model used for determination of: (a) Transverse shear modulus, G_{23} , (b) Longitudinal Young's modulus, E_{11} and Poisson's ratio, ν_{12} .

Table 2
Predicted elasticity properties for the largest RAE.

Elastic constants	K_{23} (GPa)	E_{22} (GPa)	ν_{23}	G_{23} (GPa)	E_{11} (GPa)	ν_{12}
RAE irregular fibre arrangement	8.32	12.11	0.28	4.85	146.26	0.23
RAE regular fibre arrangement	8.36	12.36	0.28	4.73	146.26	0.23
Voigt and Reuss ^a [4]	93.37 (6.77)	149.16 (8.88)	0.25 (0.23)	62.10 (3.30)	149.16 (8.88)	0.25 (0.23)
Hashin and Rosen [16]	8.73	12.72	0.27	5.01	149.17	0.23
Halpin and Tsai [17]	13.95	20.31	0.29	7.87	148.3	0.23
Whitney and Riley [18]	6.27	9.13	0.25	3.65	149.16	0.23
Experiment	–	–	–	–	138.26 ± 5.26	0.23 ± 0.01

^a Numbers in parentheses indicate lower bounds.

6. Concluding remarks

The present paper deals with the estimation of the transversely isotropic elasticity properties of a unidirectionally fibre-reinforced material. Computational modelling was used to replicate the irregular fibre arrangement of the cross section of a unidirectionally fibre-reinforced material as determined from SEM data. The results of the research indicate that a minimum representative area element of the cross section is necessary to accurately model the transverse elasticity properties. Guided by the results of the transverse elasticity properties, the computational simulations were extended to determine the longitudinal properties of the unidirectionally fibre-reinforced material with an irregular fibre arrangement. The computational estimates for the effective elastic parameters of a composite compare well with established theoretical estimates. The research also considered computational simulations of both regularly and irregularly arranged fibres in the transverse cross section of a unidirectionally reinforced composite. The theoretical relationships of Hashin and Rosen [16] provide accurate estimates of the elastic constants for the composite with an irregular fibre arrangement, provided that the representative area element considered (i.e. cross sectional area of the fibre groupings to the cross sectional area of an individual fibre) is approximately greater than 65. This estimate is also applicable for the regular fibre arrangement and is almost always satisfied in unidirectionally fibre-reinforced composites used in engineering applications.

Acknowledgements

The work described in the paper was supported by a NSERC Discovery Grant awarded to A.P.S. Selvadurai. The composite plates used in this research were supplied by Aerospace Composite Products, CA, USA. The interest and support of Mr. Justin Sparr of ACP is

gratefully acknowledged. The SEM characterisation of the composites was performed at the Materials Laboratory of Ecole Polytechnique, Montréal, Québec, Canada.

References

- [1] Jones RM. Mechanics of composite materials. J Mech Phys Solids 1987;16: 13–31.
- [2] Beaumont PWR. Fracture mechanisms in fibrous composite. In: Smith RA, editor. Fracture mechanics: current status and future prospects. New York, USA: Pergamon Press; 1979.
- [3] Spencer AJM. Deformations of fibre reinforced materials. Oxford, UK: Clarendon Press; 1972.
- [4] Christensen RM. Mechanics of composite materials. New York, USA: John Wiley & Sons; 1979.
- [5] Selvadurai APS. On the mode I stress intensity factor for an external circular crack with fibre bridging. J Comp Struct 2010;92:1512–6.
- [6] Selvadurai APS. Crack-bridging in a unidirectionally fibre-reinforced plate. J Eng Math 2010;68:5–14.
- [7] Yang S, Tewari A, Gokhale AM. Modeling of non-uniform spatial arrangement of fibers in a ceramic matrix composite. Acta Mater 1997;45:3059–69.
- [8] Hull D. An introduction to composite materials. Cambridge, UK: Cambridge University Press; 1996.
- [9] Gonzalez C, Llorca J. Multiscale modeling of fracture in fiber-reinforced composites. Acta Mater 2006;54:4171–81.
- [10] Sansalone V, Trovalusci P, Cleri F. Multiscale modeling of materials by a multifield approach: microscopic stress and strain distribution in fiber-matrix composites. Acta Mater 2006;54:3845–92.
- [11] Trias D, Costa J, Turon A, Hurtado JE. Determination of the critical size of a statistical representative volume element (SRVE) for carbon reinforced polymers. Acta Mater 2006;54:3471–84.
- [12] Goldstein J, Newbury DE, Joy DC, Lyman CE, Echlin P, Lifshin E, et al. Scanning electron microscopy and x-ray microanalysis. New York, US: Springer; 2003.
- [13] ASTM D3039. Standard test method for tensile properties of polymer matrix composite materials; 2008.
- [14] Hill R. Elastic properties of reinforced solids: Some theoretical principles. J Mech Phys Solids 1963;11:357–72.
- [15] Hill R. A self-consistent mechanics of composite materials. J Mech Phys Solids 1965;13:213–22.
- [16] Hashin Z, Rosen BW. The elastic moduli of fibre-reinforced materials. J Appl Mech 1964;31:223–32.

- [17] Halpin JC, Tsai SW. US Air Force materials laboratory report, AFML-TR. 1969; 67.
- [18] Whitney JM, Riley MB. Elastic properties of fibre reinforced composite materials. *AIAA J* 1966;4:1537–42.
- [19] Spencer AJM. The transverse moduli of fibre-composite materials. *J Comp Sci Technol* 1986;27:93–109.
- [20] Sideridis E. The transverse elastic modulus of fibre-reinforced composites as defined by concept of interphase. *J Appl Polymer Sci* 1993;48:243–55.
- [21] Sun CT, Vaidya RS. Prediction of composite properties from a representative volume element. *J Comp Sci Technol* 1996;56:171–9.
- [22] Selvadurai APS. *Partial differential equations in mechanics. The Biharmonic equation, Poisson's equation, vol. 2.* Berlin, Germany: Springer-Verlag; 2000.